Investigation of Solid–Gas Reaction Heat Transformer System with the Consideration of Multistep Reactions

C. Wang, P. Zhang, and R. Z. Wang
Institute of Refrigeration and Cryogenics, Shanghai Jiao Tong University, Shanghai 200240, China

DOI 10.1002/aic.11560
Published online July 8, 2008 in Wiley InterScience (www.interscience.wiley.com).

The performance of solid–gas reaction heat transformer system using $MnCl_2$ and $CaCl_2$ was investigated with the consideration of multistep reactions between $CaCl_2$ and NH_3. The reactions between $CaCl_2$ and NH_3 could be $CaCl_2{\cdot}2/4NH_3$ and $CaCl_2{\cdot}4/8NH_3$. The simulated results were verified by the experimental data. From the analysis results, it was concluded that the two reactions between $CaCl_2$ and NH_3 existed simultaneously. The favored conditions for the simultaneous occurrence of multistep reactions were discussed. The main reaction in the system with the initial state of $CaCl_2{\cdot}2NH_3$ and $CaCl_2{\cdot}4NH_3$ were designated as the reaction of $CaCl_2{\cdot}2/4NH_3$ and $CaCl_2{\cdot}4/8NH_3$, respectively. It was concluded that high driving temperature T_M, large relative gas volume, and large specific heat transfer area were the favored conditions for the simultaneous occurrence of multistep reactions in the systems both with the initial state of $CaCl_2{\cdot}2NH_3$ and $CaCl_2{\cdot}4NH_3$. High initial charging pressure P_0 was favored for the system with the initial state of $CaCl_2{\cdot}2NH_3$, while low P_0 was favored for the system with the initial state of $CaCl_2{\cdot}4NH_3$. The impacts of the simultaneous occurrence of multistep reactions on the system performance indicators [temperature lift, specific power, and system coefficient of performance (COP)] were also investigated in this article. It was concluded that the occurrence of the reaction of $CaCl_2{\cdot}4/8NH_3$ for the initial state of $CaCl_2{\cdot}2NH_3$ led to better system performance, i.e., larger temperature lift, larger specific power, and larger system COP. However, the occurrence of the reaction of $CaCl_2{\cdot}2/4NH_3$ for the initial state of $CaCl_2{\cdot}4NH_3$ would lead to lower specific power. The temperature lift and system COP were larger for the initial state of $CaCl_2{\cdot}4NH_3$; while the cycle period was shorter for the initial state of $CaCl_2{\cdot}2NH_3$. *AIChE J,* 54: 2464–2478, 2008
Keywords: solid–gas reaction, heat transformer system, multistep reaction

Introduction

The energy consumption and environmental pollution have urged the researchers to explore new green energy sources and improve energy consumption efficiency.[1–3] In many industries, large amount of waste heat is released to the environment, causing environmental pollution. As a matter of fact, the temperature of the waste heat from industries could be as high as 100°C or even higher. It is simply released and wasted, because only the higher temperature heat is useful in the industrial process. Thus, attempt to recover the waste heat and possibly upgrade the waste heat to higher temperature could be interesting, as it will reduce the industrial cost and protect the environment. Heat transformers, which could

Correspondence concerning this article should be addressed to P. Zhang at zhangp@sjtu.edu.cn.

be driven by the waste heat and generate heat at higher temperature,[4] are therefore promising for industrial application.

Heat transformer systems can be categorized into three types: absorption, adsorption, and solid–gas reaction systems. Among these three systems, the solid–gas reaction heat transformer system has the following merits over the other two systems: (1) no crystallization and solution corrosion problems, which are usually experienced in the absorption system; (2) larger amount of reaction heat compared with that of absorption and adsorption systems; (3) adaptability to the wide range of operation temperature, especially at high temperature where absorption/adsorption system could not be used. Moreover, the reactive gas used in the solid–gas reaction heat transformer system is environment-friendly, such as H_2, H_2O, and NH_3 (GWP and ODP are zero). Therefore, the solid–gas reaction heat transformer system is believed to have commercial value and potential application.

The heat transformer system is a type of heat pump, and its working principle is shown in Figure 1. As seen in Figure 1a (the thermodynamic diagram), the heat transformer system degrades part of the input heat (part 1) from the medium temperature T_M to the low temperature T_L, where T_M might be the temperature of the waste heat (the driving temperature) and T_L might be the ambient temperature. The work capacity generated from the degradation from T_M to T_L can then be used for raising the other part of input heat (part 2) from T_M to the high temperature T_H. For the solid–gas reaction heat transformer, the system operation principle is shown in Figure 1b (Clausius-Clapeyron diagraph). The working pair could be metal chloride/NH_3, metal hydride/H_2, and metal oxide/CO_2 or H_2O. The system shown in Figure 1b is the single-stage solid–gas reaction heat transformer, and composed of two salts: the low temperature salt S_L and the high temperature salt S_H.

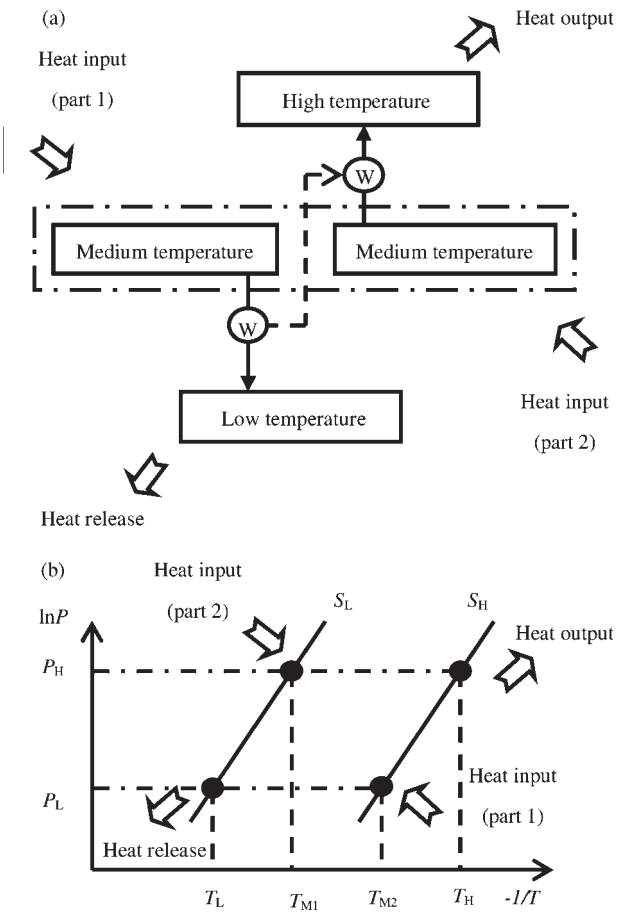

Figure 1. Principle of the system operation.

(a) Thermodynamic sketch for the heat transformer system; (b) Clausius-Clapeyron diagraph for the single-stage solid–gas reaction heat transformer system. (T_{M1} and T_{M2} in Figure 1b could be the same).

The two lines in Figure 1b represent the equilibrium status for the solid–gas reaction, which was determined by Eq. 1. The system operation is composed of two processes: the low pressure process P_L and the high pressure process P_H. During the low pressure process (P_L), the salt S_L is synthesized at T_L and the salt S_H is decomposed at T_{M2}. In the other process (P_H), the salt S_L is decomposed at T_{M1} and the salt S_H is synthesized at T_H. The work capacity in Figure 1a is then the chemical potential stored in the decomposed salt S_H. During the synthesis of the salt S_H, the chemical potential is released, generating heat at T_H. In this article, the temperatures T_{M1} and T_{M2} were chosen as same as T_M. The difference between T_M and T_H was then the temperature lift ΔT, which was one major indicator for the performance of heat transformer system.

$$\ln(P_{eq}) = -\frac{H}{R}\cdot\frac{1}{T_s} + \frac{S}{R} \tag{1}$$

The performance of solid–gas reaction heat transformer system has been investigated by many authors.[5–7] Influences of several factors, such as the driving temperature T_M, the ambient temperature T_L, and the inner irreversibility, etc, have been widely analyzed. Some experimental systems were made and their performances were tested. However, most of the researchers neglected the possible multistep reactions between the reactive salt and the gas. For instance, the reaction between $MnCl_2$ and NH_3 involves three steps, and the reaction between $CaCl_2$ and NH_3 involves four steps, which are given by Eqs. 2 and 3. The design of the solid–gas reaction heat transformer system was usually based on a single reaction, such as those given by Eqs. 2c and 3c. However, other reactions, i.e., Eqs. 2a, 2b, 3a, 3b, and 3d, might also occur during the system operation. Therefore, the reaction between the reactive salt and the gas might not be the single reaction as that adopted in the system design, but the simultaneous occurrence of multistep reactions, which differed from the designed condition. Moreover, the simultaneous occurrence of multistep reactions might have other influences on the system operation and system performance. Unfortunately, little researches have been carried out on this topic.

For $MnCl_2$

$$MnCl_2 + NH_3 \Leftrightarrow MnCl_2 \bullet NH_3 \tag{2a}$$

$$MnCl_2 \bullet NH_3 + NH_3 \Leftrightarrow MnCl_2 \bullet 2NH_3 \tag{2b}$$

$$MnCl_2 \bullet 2NH_3 + 4NH_3 \Leftrightarrow MnCl_2 \bullet 6NH_3 \tag{2c}$$

For $CaCl_2$

$$CaCl_2 + NH_3 \Leftrightarrow CaCl_2 \bullet NH_3 \quad (3a)$$

$$CaCl_2 \bullet NH_3 + NH_3 \Leftrightarrow CaCl_2 \bullet 2NH_3 \quad (3b)$$

$$CaCl_2 \bullet 2NH_3 + 2NH_3 \Leftrightarrow CaCl_2 \bullet 4NH_3 \quad (3c)$$

$$CaCl_2 \bullet 4NH_3 + 4NH_3 \Leftrightarrow CaCl_2 \bullet 8NH_3 \quad (3d)$$

In this study, the reactive salts for the solid–gas reaction heat transformer system were $MnCl_2$ as the high temperature salt S_H and $CaCl_2$ as the low temperature salt S_L, and the reactive gas was NH_3. The medium temperature T_M was 90–120°C, and the low temperature T_L was 0–30°C. As shown in Figure 1b, the decomposition temperature of the reactive salts of S_L and S_H is T_M. However, the equilibrium temperatures T_{eq} of the reactions given by Eqs. 2a, 2b, 3a, and 3b are larger than T_M. For instance, T_{eq} of the reactions of $MnCl_2 \cdot 0/1NH_3$, $MnCl_2 \cdot 1/2NH_3$, $CaCl_2 \cdot 0/1NH_3$, and $CaCl_2 \cdot 1/2NH_3$ under the pressure of 0.1 MPa are 340, 247, 226, and 173°C, respectively. Since the salt temperature T_s should be higher than T_{eq} during the decomposition process, the decomposition reactions are hard to realize. Therefore, the reactions given by Eqs. 2a, 2b, 3a and 3b would not happen in the solid–gas reaction heat transformer system in this article. The reaction between $MnCl_2$ and NH_3 was then the single reaction described by Eq. 2c. However, the reaction between $CaCl_2$ and NH_3 was still uncertain, which might be the combination of the reactions given by Eqs. 3c and 3d.

In this article, theoretical analysis on the performance of the solid–gas heat transformer system was carried out, and experimental measurement was also done for comparison. Two questions were to be answered: (1) whether or not the two reactions between $CaCl_2$ and NH_3 occurred simultaneously in the solid–gas reaction heat transformer system and what were the favored conditions for the simultaneous occurrence; (2) the impact of multistep reactions on the system performance, the indicators of which were the temperature lift ΔT, specific power, and system coefficient of performance (COP).

Experimental Set-Up

The schematic illustration of the experimental set-up of the solid–gas reaction heat transformer system is shown in Figure 2. The reactive salts in the system were $MnCl_2$ and $CaCl_2$, whereas the reactive gas was NH_3. The system was composed of three reactors: two reactors with $CaCl_2$ and the other with $MnCl_2$. Valve 1 was used for initial charging with NH_3 and for vacuum pumping, and was kept closed during system operation. Valve 2 was used to control the flow of NH_3 between the reactors and was kept open during the system operation. The temperatures of the reactors were controlled by the thermostat baths 1 and 2 (precision of temperature control: ±0.5°C). In the experiments, the temperatures of the thermostat baths were measured by K-Type thermocouples (precision: ±1°C), and the temperatures of the reactive blocks in the reactors were measured by PT1000 temperature sensors (precision: ±0.5°C). The system pressure was measured by a pressure transducer (range: 0–2.5 MPa; precision: ±1.0% FS).

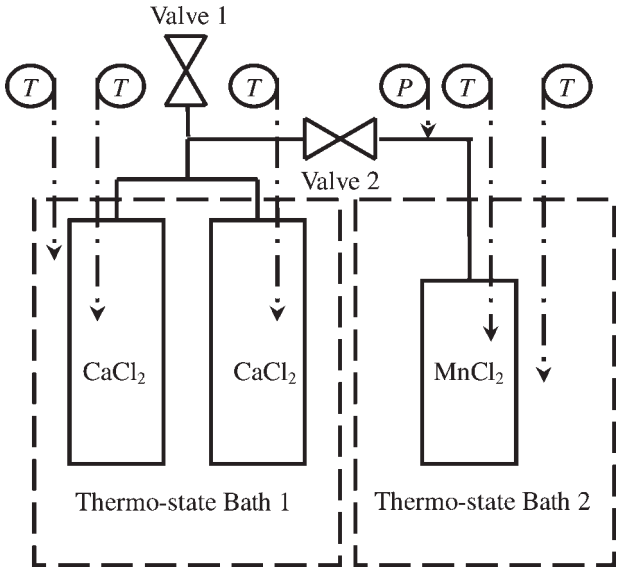

Figure 2. Experimental set-up of the solid–gas reaction heat transformer system.

Fabrication of the reactive block

It was pointed out that one major factor causing poor performance of the solid–gas reaction system was the heat or mass transfer limitation.[8,9] In the experimental set-up, enhancement of heat and mass transfer was therefore considered. As the composite reactive block was regarded as one possible method for the heat and mass transfer enhancement,[5] it was then used in the experiments. The fabrication procedure was described in detail.[9] The expandable graphite was expanded at 700°C for 15 min. The expanded graphite was then compressed into matrix at certain apparent density ρ_b. The reactive salt was later impregnated into the matrix. The expanded graphite matrix impregnated with salt was then dried to become the composite reactive block with certain mass fraction of expanded graphite f_G. In this way, the high thermal conductivity of expanded graphite matrix, which was the major structure for heat transfer, would improve the heat transfer performance of the reactive block. The porous structure of the expanded graphite matrix was also favored for the mass transfer in the reactive block. Furthermore, it could be concluded from the SEM and BEC photos that the reactive salt was dispersed and uniformly distributed in the reactive block.[9] Thus, the agglomeration phenomenon could be avoided, and the performance of the reactive block was more stable, which has also been proven by repeated experiments. In this article, the fabricated reactive block was in the shape of cylinder, and the outer diameter was 54 mm. A hole with a diameter of 20 mm was left in the center of the block for gas flow. The heights of the reactive blocks with $MnCl_2$ and $CaCl_2$ were 12 and 16 mm, respectively. The thermal conductivity[10] was larger than 10 W/(m °C), which was much larger than that of the reactive salt, i.e., 0.1–0.3 W/(m °C) and the gas permeability[11] could be higher than 10^{-15} m^2.

The thermal conductivity of the reactive block is increased with the apparent density ρ_b and the mass fraction f_G of

Table 1. Parameters of the Reactive Blocks in the Experimental Set-Up

Apparent Density of Expanded Graphite ρ_b (kg/m^3)		Mass Fraction of Expanded Graphite f_G		Porosity of the Reactive Block				
				$CaCl_2 \cdot yNH_3$			$MnCl_2 \cdot yNH_3$	
$CaCl_2$	$MnCl_2$	$CaCl_2$	$MnCl_2$	2	4	8	2	6
200	200	0.5	0.4	0.68	0.60	0.46	0.72	0.53

expanded graphite.[11] However, the gas permeability is decreased with ρ_b and increased with f_G. Moreover, the mass transfer limitation is more likely to happen under low pressure. In the experiments, the salts of $MnCl_2$ and $CaCl_2$ were used. As shown in Figure 1b, during the system operation, the salt of $MnCl_2$ is synthesized at high pressure P_H and is decomposed at low pressure P_L; while the salt of $CaCl_2$ is decomposed at high pressure P_H and is synthesized at low pressure P_L. Therefore, more care should be taken in the mass transfer performance of reactive block with $CaCl_2$.

The apparent density ρ_b and the mass fraction f_G of the reactive blocks are listed in Table 1. The porosities of reactive blocks, which were calculated by Eq. 4,[12] are also listed in this table for reference.

$$\varepsilon = 1 - \frac{\rho_b}{\rho_G} - \frac{1 - f_G}{f_G} \cdot \frac{\rho_b \cdot MV_s}{MW_s} \tag{4}$$

where ρ_G was the real density of expanded graphite, which was 2260 kg/m^3.

Initial charging of experimental set-up

In the case of the solid–gas reaction heat transformer system designed with the reactions of $CaCl_2 \cdot 2/4NH_3$ and $MnCl_2 \cdot 2/6NH_3$, the initial state of $MnCl_2$ was $MnCl_2 \cdot 6NH_3$ and the initial state of $CaCl_2$ was $CaCl_2 \cdot 2NH_3$. While in the case of the solid–gas reaction heat transformer system designed with the reactions of $CaCl_2 \cdot 4/8NH_3$ and $MnCl_2 \cdot 2/6NH_3$, the initial states of $MnCl_2$ and $CaCl_2$ should be $MnCl_2 \cdot 6NH_3$ and $CaCl_2 \cdot 4NH_3$, respectively. However, it was more likely to obtain $CaCl_2 \cdot 8NH_3$ when charging $CaCl_2$ at ambient temperature T_L with NH_3 at high pressure. Therefore, the initial charging of the experimental set-up in this article was composed of two steps, which are shown in Figure 3. The first step is expressed in Figure 3a; where the reactive blocks with $MnCl_2$ and $CaCl_2$ were charged with NH_3 at high pressure. The valves 1 and 2 were open, and the reactors were at ambient temperature T_L. At the end of this step, the states of $MnCl_2$ and $CaCl_2$ were $MnCl_2 \cdot 6NH_3$ and $CaCl_2 \cdot 8NH_3$, respectively. As shown in Figure 3b, the valve 2 is closed in the next step. The reactor with $CaCl_2 \cdot 8NH_3$ was decomposed at the initial charging temperature T_0. The constraint pressure was regulated at 0.1 MPa. At the end of this step, the state of $CaCl_2$ would be the initial states, which was $CaCl_2 \cdot 2NH_3$ or $CaCl_2 \cdot 4NH_3$, depending on T_0. Then, the valve 1 was closed during the experiments. In this way, the initial states of $MnCl_2$ and $CaCl_2$ for the designed system operation could be achieved.

The initial charging temperature T_0 could be determined from the Clausius-Clapeyron diagram, as shown in Figure 4.

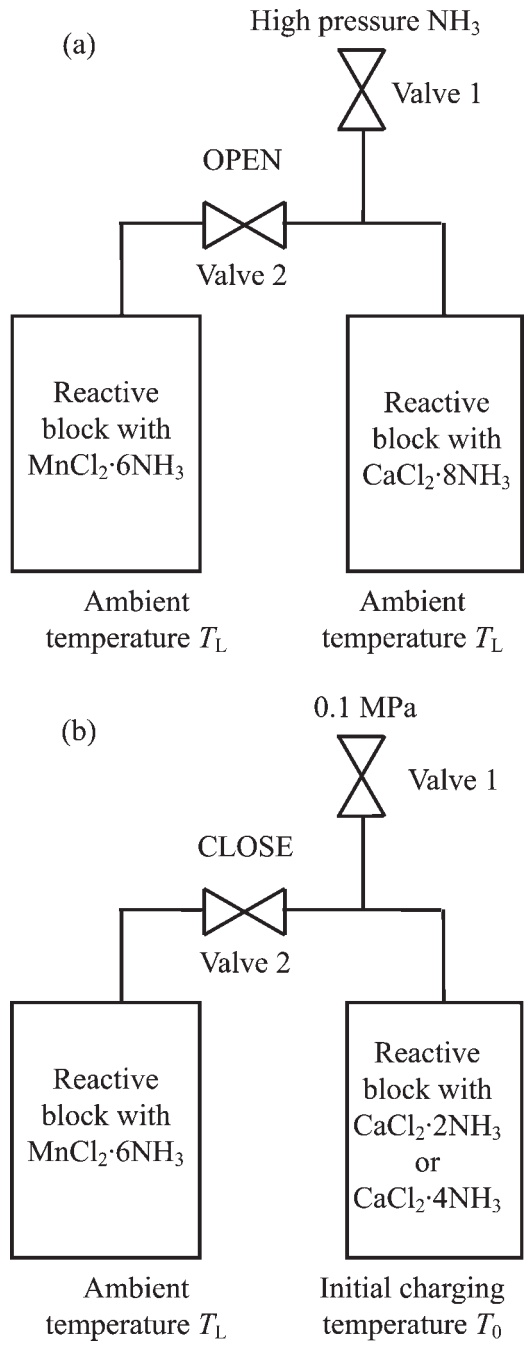

Figure 3. Schematic illustration of the initial charging process of the experimental set-up.

(a) Final status of the first step; (b) Final status of the second step.

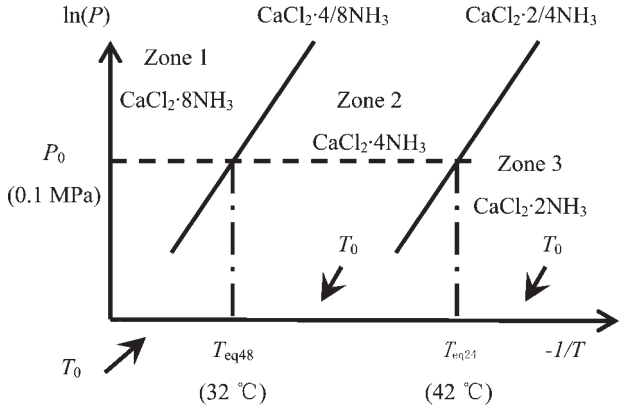

Figure 4. Clausius-Clapeyron diagram of the reactions of $CaCl_2$·2/4NH_3 and $CaCl_2$·4/8NH_3.

The left line represents the equilibrium status of the reaction of $CaCl_2$·4/8NH_3 and the right one represents that of the reaction of $CaCl_2$·2/4NH_3. The two lines divide the area into three zones: zone 1 ($CaCl_2$·8NH_3), zone 2 ($CaCl_2$·4NH_3), and zone 3 ($CaCl_2$·2NH_3). Given the initial charging pressure P_0 at 0.1 MPa, the equilibrium temperatures of the reactions of $CaCl_2$·2/4NH_3 and $CaCl_2$·4/8NH_3 are T_{eq24} (42°C) and T_{eq48} (32°C), respectively. Therefore, when T_0 was between 32 and 42°C, the initial state of $CaCl_2$ was $CaCl_2$·4NH_3; and when T_0 was higher than 42°C, the initial state of $CaCl_2$ was $CaCl_2$·2NH_3.

System operation

The system operation is expressed in Figure 5. The valve 1 was kept closed and the valve 2 was kept open in experiments. Thus, the valves are not shown in Figure 5. As mentioned earlier, the system operation comprised of two steps: the high pressure process P_H and the low pressure process P_L. Since the initial state of $MnCl_2$ is $MnCl_2$·6NH_3, the first step would be the decomposition of $MnCl_2$ and the synthesis of $CaCl_2$, as shown in Figure 5a. The decomposition temperature of $MnCl_2$ was T_M, and the synthesis temperature of $CaCl_2$ was T_L. The period of this step was about 120 min to make sure the completion of the solid–gas reactions. The next step is then the decomposition of $CaCl_2$ and the synthesis of $MnCl_2$, as shown in Figure 5b. The decomposition temperature of $CaCl_2$ was T_M and the synthesis temperature of $MnCl_2$ was T_H. This was also the process in which the high temperature heat was generated. The period of this step was about 30 min. Then the cycle of system operation was repeated under each experimental condition. The histories of the salt temperatures during system operation were recorded.

Theoretical Analysis

In the experimental set-up shown in Figure 2, only the salt temperatures (block temperatures) and the gas pressure were measured in experiments. As the solid–gas reaction in the heat transformer system could not be directly measured, only theoretical analysis was carried out in this article, which was based on the principles of energy and mass conservation. The theoretical analysis results of the salt temperatures T_s in the reactors with $MnCl_2$ and $CaCl_2$ were also compared with the experimental results.

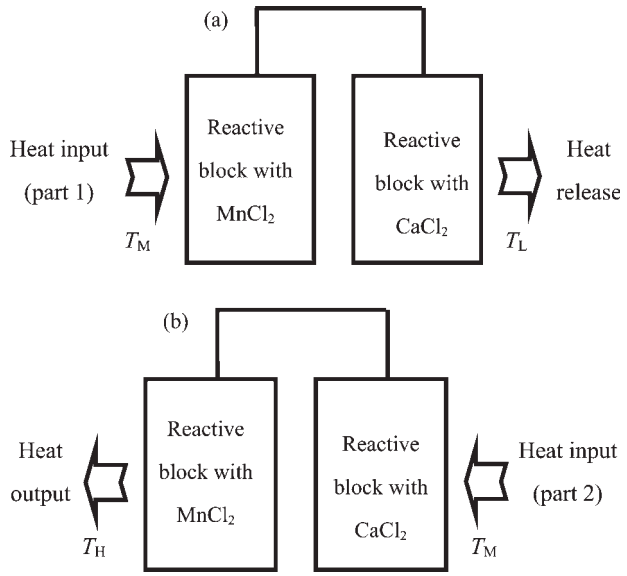

Figure 5. Schematic illustration of the system operation.

Physical model

The physical model of the solid–gas reaction heat transformer system in the theoretical analysis is shown in Figure 6. It is composed of three portions: the reactor with $MnCl_2$, the reactor with $CaCl_2$, and the gas tank connecting the two reactors. The reactor is composed of the reactive block and the metal vessel; and the gas tank is filled with NH_3. Heat is added to and exported from the reactors by the convection of heat transfer fluid. Because the thermal conductivity of the reactive block was larger than 10 W/(m °C), and the gas permeability was larger than 10^{-15} m^2, minimal heat and mass transfer limitations in the block were expected. The salt temperature T_s and the gas pressure P were assumed uniformly distributed in the reactive block. Consequently, the reaction degree x was also uniformly distributed. Additionally, the temperature of the metal vessel was regarded to be the same as that of the reactive block. Therefore, lumped parameters for the salt temperature T_s, the gas pressure P, and the reac-

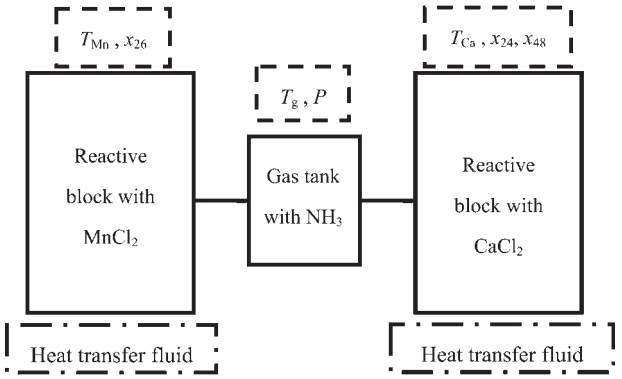

Figure 6. Physical model in the theoretical analysis.

Table 2. Operation Conditions of the Solid–Gas Reaction Heat Transformer System

Process	Reactor with the Reactive Salt	The Temperature of Heat Transfer Fluid T_f
Low pressure P_L	$MnCl_2$	Medium temperature T_M
	$CaCl_2$	Low temperature T_L
High pressure P_H	$MnCl_2$	Medium temperature T_M
	$CaCl_2$	Medium temperature T_M

tion degree x were considered in the theoretical analysis, and NH_3 was treated as ideal gas.

For the reactor with $MnCl_2$, only the single reaction of $MnCl_2{\cdot}2/6NH_3$ occurred during the system operation. Thus, the salt temperature T_{Mn} and the reaction degree x_{26} for the reaction of $MnCl_2{\cdot}2/6NH_3$ were considered. As for the reactor with $CaCl_2$, the reactions of $CaCl_2{\cdot}2/4NH_3$ and $CaCl_2{\cdot}4/8NH_3$ might happen. Therefore, the salt temperature T_{Ca}, the reaction degree x_{24} for the reaction of $CaCl_2{\cdot}2/4NH_3$, and the reaction degree x_{48} for the reaction of $CaCl_2{\cdot}4/8NH_3$ were taken into consideration. The gas temperature T_g and the gas pressure P were also calculated in the theoretical analysis, the constraint pressures in the reactors with $MnCl_2$ and $CaCl_2$ were the same as the gas pressure P.

The operation conditions of the solid–gas reaction heat transformer system are listed in Table 2. In the low pressure process P_L, the temperatures of the heat transfer fluids for the reactors with $MnCl_2$ and $CaCl_2$ were T_M and T_L, respectively; while in the high pressure process P_H, the temperatures of heat transfer fluids were T_M for both reactors.

Numerical model

Energy and Mass Conservation. Based on the principles of energy and mass conservation, the salt temperature T_s and the gas temperature T_g were determined. The variation of T_s was due to two parts: (1) the heat transfer between the reactive block and the heat transfer fluid and (2) the heat consumption or generation in solid–gas reaction within the reactive block. Thus, the equation of T_s is formulated as Eq. 5a.

$$(\rho \cdot C) \cdot \frac{dT_s}{dt} = \frac{U \cdot A}{V_B} \cdot (T_f - T_s) + S \tag{5a}$$

Because NH_3 was thermally equilibrated with the reactive salt, the variation of T_g was then due to the mixing of the hot NH_3 gas emitted from the decomposition process and NH_3 in the gas tank shown in Figure 6. Thus, the equation of T_g is formulated as Eq. 5b.

$$n_g \cdot \frac{dT_g}{dt} = \frac{dn_{dec}}{dt} \cdot (T_s - T_g)_{dec} \tag{5b}$$

where the term "A/V_B" in Eq. 5a was defined as the specific heat transfer area, and the source term "s" in Eq. 5a was related to the reaction rate in the reactive block. The relationship could be described by Eq. 5c.

$$s = v \cdot \frac{n_s}{V_B} \cdot H \cdot \frac{dx}{dt} \tag{5c}$$

As mentioned earlier, during the system operation, one reactive salt (e.g., $CaCl_2$) was synthesized, while the other reactive salt (e.g., $MnCl_2$) was decomposed. The variation of gas amount in the gas tank was then related to the synthesis rate (e.g., $CaCl_2$) and the decomposition rate (e.g., $MnCl_2$). Since NH_3 was consumed in the synthesis process and generated in the decomposition process, the molar amount of NH_3 in the gas volume is then calculated from Eq. 6, based on the principle of mass conservation.

The gas temperature T_g and molar amount n_g are given in Eqs. 5b and 6, respectively. Because NH_3 was treated as ideal gas, the gas pressure P is then derived from Eq. 7. The ratio of gas volume to the total volume of the reactive blocks was V_g/V_B, and it was defined as the relative gas volume.

$$\frac{dn_g}{dt} = \frac{dn_{dec}}{dt} - \frac{dn_{sys}}{dt} \tag{6a}$$

$$\frac{dn_{dec}}{dt} = \left(n_s \cdot v \cdot \left|\frac{dx}{dt}\right|\right)_{dec} \tag{6b}$$

$$\frac{dn_{syn}}{dt} = \left(n_s \cdot v \cdot \left|\frac{dx}{dt}\right|\right)_{syn} \tag{6c}$$

$$\frac{dP}{dt} = \frac{R}{V_g} \cdot \left(\frac{dn_g}{dt} \cdot T_g + n_g \cdot \frac{dT_g}{dt}\right) \tag{7}$$

Solid–Gas Reaction. As mentioned earlier, for the salt of $MnCl_2$ in the solid–gas reaction heat transformer system, the single reaction of $MnCl_2{\cdot}2/6NH_3$ occurred. When the salt temperature T_{Mn} of $MnCl_2$ was lower than the equilibrium temperature T_{eq26} corresponding to the gas pressure P, the synthesis of the reaction occurred. When T_{Mn} was higher than T_{eq26}, the decomposition reaction occurred. The reaction degree x_{26} is determined by Eq. 8a.

$$x_{26} = \frac{n_{MnCl_2 \bullet 6NH_3}}{n_{MnCl_2 \bullet 2NH_3} + n_{MnCl_2 \bullet 6NH_3}} \tag{8a}$$

However, for the salt of $CaCl_2$, two reactions might happen in the system. As shown in Figure 4, the Clausius-Clapeyron diagram is divided into three zones, where the states of $CaCl_2$ in zones 1, 2, and 3 are $CaCl_2{\cdot}8NH_3$, $CaCl_2{\cdot}4NH_3$, and $CaCl_2{\cdot}2NH_3$, respectively. Therefore, the reaction between $CaCl_2$ and NH_3 was determined by the salt temperature T_{Ca} of $CaCl_2$ and the gas pressure P. Given the gas pressure P, the equilibrium temperatures for the reactions of $CaCl_2{\cdot}2/4NH_3$ and $CaCl_2{\cdot}4/8NH_3$ are T_{eq24} and T_{eq48}, respectively. The reactions in zones 1, 2, and 3 are then listed in Table 3. When the salt temperature T_{Ca} was lower than T_{eq48}, both synthesis reactions occurred; when T_{Ca} ranged between T_{eq48} and T_{eq24}, the decomposition of the reaction of $CaCl_2{\cdot}4/8NH_3$ and the synthesis of the reaction of $CaCl_2{\cdot}2/4NH_3$ occurred; and when T_{Ca} was higher than T_{eq24}, both decomposition reactions occurred. The reaction degrees x_{24} and x_{48} are determined by Eqs. 8b and 8c, respectively.

$$x_{24} = \frac{n_{CaCl_2 \bullet 2NH_3}}{n_{CaCl_2 \bullet 2NH_3} + n_{CaCl_2 \bullet 4NH_3}} \tag{8b}$$

$$x_{48} = \frac{n_{CaCl_2 \bullet 8NH_3}}{n_{CaCl_2 \bullet 4NH_3} + n_{CaCl_2 \bullet 8NH_3}} \tag{8c}$$

Reaction Rate. As shown in Eqs. 5 and 6, the salt temperature T_s and the gas pressure P were related to the reac-

Table 3. Solid–Gas Reaction Between $CaCl_2$ and NH_3 (Given Gas Pressure P)

Salt Temperature T_{Ca}	The Reaction of $CaCl_2 \cdot 2/4NH_3$	The Reaction of $CaCl_2 \cdot 4/8NH_3$
$T_{Ca} < T_{eq48}$	Synthesis	Synthesis
$T_{eq48} < T_{Ca} < T_{eq24}$	Synthesis	Decomposition
$T_{Ca} > T_{eq24}$	Decomposition	Decomposition

tion rate. The reaction rate equation has been widely investigated,[13–16] and that of $MnCl_2 \cdot 2/6NH_3$ has been concluded in Han et al.[16] In this article, the reaction rates for the reactions of $CaCl_2 \cdot 2/4NH_3$ and $CaCl_2 \cdot 4/8NH_3$ were measured with the experimental set-up.[17] The reaction rate equations are fitted in the form of Eq. 9. As shown in this equation, the reaction rate was related to the reaction degree x, the constants a and b, the salt temperature T_s, and the gas pressure P. The parameters a and b are listed in Table 4.

For synthesis

$$\frac{dx}{dt} = a \cdot (1-x)^b \cdot \left(1 - \frac{P_{eq}}{P}\right) \tag{9a}$$

For decomposition

$$\frac{dx}{dt} = a \cdot x^b \cdot \left(1 - \frac{P_{eq}}{P}\right) \tag{9b}$$

where P_{eq} was the equilibrium pressure determined by Eq. 1.

Initial Conditions. The initial charging state of the experimental set-up was $MnCl_2 \cdot 6NH_3$, and $CaCl_2 \cdot 2NH_3$ or $CaCl_2 \cdot 4NH_3$. The measurement was started after the experimental set-up was thermally equilibrated with the ambient temperature T_L. Thus, the initial conditions are determined by Eq. 10.

For the reactor with $MnCl_2$

$$T_{Mn} = T_L \tag{10a}$$

$$x_{26} = 1 \tag{10b}$$

For the reactor with $CaCl_2$

$$T_{Ca} = T_L \tag{10c}$$

For the initial state of $CaCl_2 \cdot 2NH_3$

$$x_{24} = 1 \tag{10d}$$

$$x_{48} = 0 \tag{10e}$$

For the initial state of $CaCl_2 \cdot 4NH_3$

$$x_{24} = 0 \tag{10f}$$

$$x_{48} = 0 \tag{10g}$$

For NH_3

$$T_g = T_L \tag{10h}$$

$$P = P_0 \tag{10i}$$

Results and Discussion

Two typical examples of the experimental and theoretical results of the salt temperatures T_s are shown in Figure 7. The results for the initial state of $CaCl_2 \cdot 4NH_3$ are shown in Figures 7a, b. The results for the initial state of $CaCl_2 \cdot 2NH_3$ are shown in Figures 7c, d.

In Figures 7a, b, the experimental and theoretical results for the initial state of $CaCl_2 \cdot 4NH_3$ are depicted, respectively. In the period of 0–3000 s, the reactor with $MnCl_2$ was heated at 120°C, and the reactor with $CaCl_2$ was cooled at 30°C. Since the initial states of $CaCl_2$ and $MnCl_2$ in the system were $CaCl_2 \cdot 4NH_3$ and $MnCl_2 \cdot 6NH_3$, respectively, the salt of $MnCl_2$ was decomposed and the salt of $CaCl_2$ was synthesized in this period. As the synthesis reaction is exothermic, the salt temperature T_{Ca} increased at the beginning. The later decrease of the salt temperature T_{Ca} was due to heat rejection to T_L.

In the next step, the salt of $CaCl_2$ was decomposed and the salt of $MnCl_2$ was synthesized. This step took about 30 min. The heating temperature of the reactor with $CaCl_2$ and the cooling temperature of the reactor with $MnCl_2$ were both at 120°C. The heat released during the synthesis of $MnCl_2$ and NH_3 lifted the salt temperature T_{Mn} to about 145°C. As the reaction proceeded, the synthesis rate of the reaction of $MnCl_2 \cdot 2/6NH_3$ became smaller. Thus, the salt temperature T_{Mn} was decreased, because of the cooling of the heat transfer fluid.

During the period 5000–12,000 s, the reactor with $CaCl_2$ was cooled at the ambient temperature T_L. In this process, the heat transfer fluid for the reactor with $MnCl_2$ was at T_M. As Figure 7a depicts, in the first few minutes, the salt temperature T_{Mn} of $MnCl_2$ was still higher than T_M. Therefore, the salt of $MnCl_2$ was also cooled down by the heat transfer fluid around the reactor. There was no decomposition reaction of $MnCl_2 \cdot 2/6NH_3$.

The cooling of the salt of $CaCl_2$ slows down at around 7000 s in the experiment, as shown in Figure 7a. This was also found in the next cycle at about 17,000 s. It could be explained by the variation of the reaction degrees x with time. In Figure 8b, x_{24} decreased and x_{48} increased at this moment. Thus, synthesis of the reactions of $CaCl_2 \cdot 2/4NH_3$ and $CaCl_2 \cdot 4/8NH_3$ occurred from this time on. Since the synthesis reactions are exothermic, the cooling of the reactor with $CaCl_2$ slowed down. Similar results are also found in Figure 7b, which depicts the results of the theoretical analysis.

In Figures 7c, d, the experimental and theoretical results of the salt temperatures T_{Ca} and T_{Mn} are compared. T_M was 105°C and T_L was 25°C. The experimentally measured tem-

Table 4. Parameters a and b in the Reaction Rate Equations

	Synthesis		Decomposition	
	a	b	a	b
The reaction of $CaCl_2 \cdot 2/4NH_3$	0.0287	1.78	0.0045	0.468
The reaction of $CaCl_2 \cdot 4/8NH_3$	0.0125	2.104	0.0195	1.005

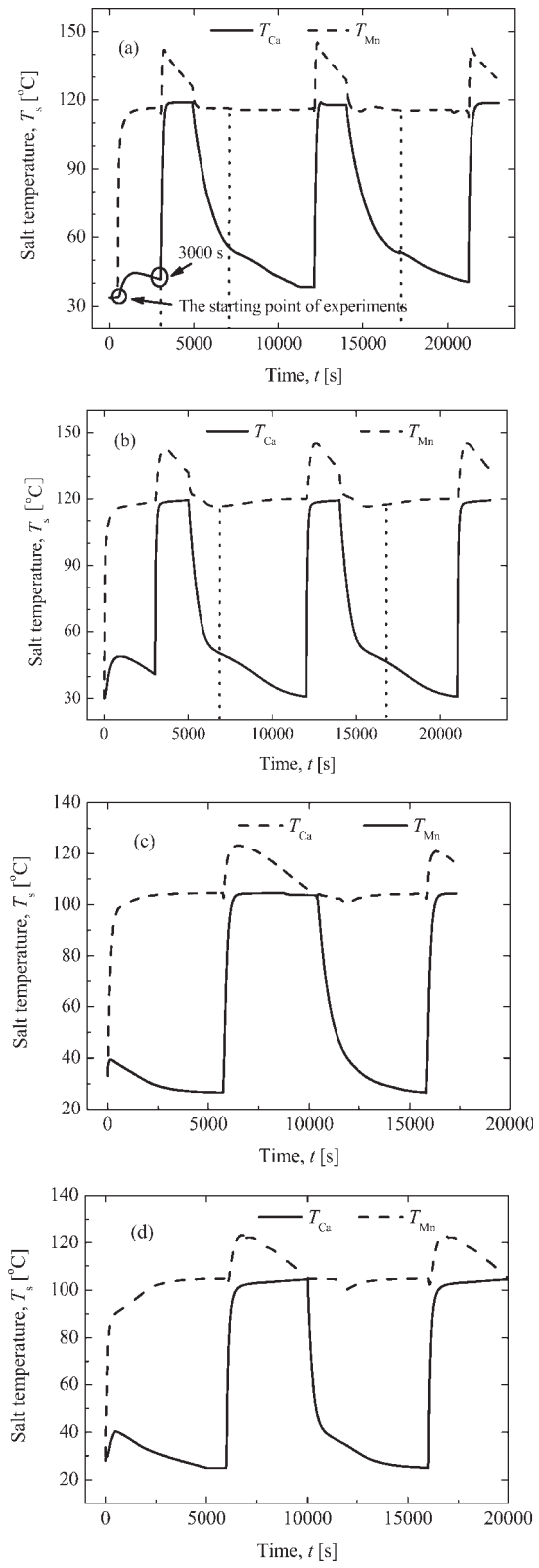

Figure 7. Typical examples of the experimental and theoretical results.

(a) Experimental result and (b) theoretical result for the initial state of $CaCl_2 \cdot 4NH_3$ (T_M and T_L were 120 and 30°C, respectively); (c) experimental result and (d) theoretical result for the initial state of $CaCl_2 \cdot 2NH_3$. (T_M and T_L were 105 and 25°C, respectively).

perature lift ΔT was 18°C, while the theoretical result was 19°C. The results of ΔT under different operation conditions are listed in Table 5. From Figure 7 and Table 5, it was concluded that the theoretical results agreed well with the experimental results. Since the heat loss during system operation was not considered in the theoretical analysis, there was

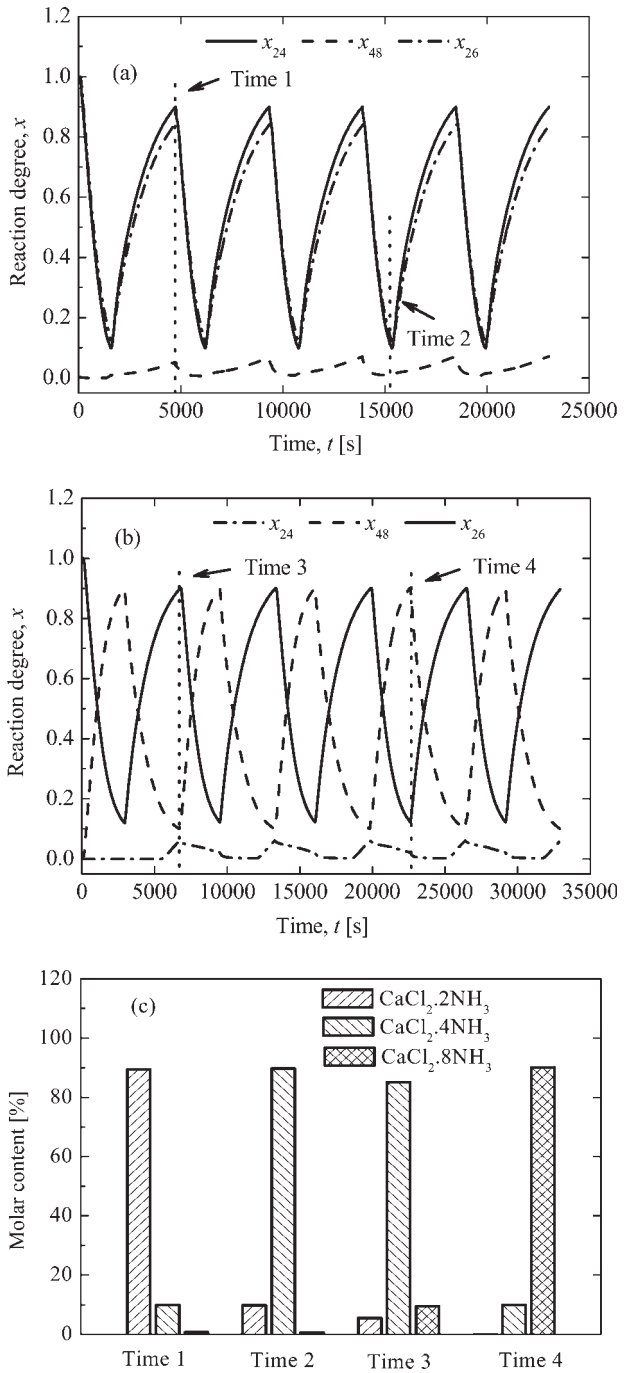

Figure 8. Reaction degrees in the solid–gas reaction heat transformer system.

(a) Variations of reaction degrees for the initial state of $CaCl_2 \cdot 2NH_3$; (b) variations of reaction degrees for the initial state of $CaCl_2 \cdot 4NH_3$; (c) molar content of $CaCl_2$ in the reactive block.

Table 5. The Theoretical and Experimental Results on the Temperature Lift ΔT

The Initial State of $CaCl_2$	T_M (°C)	T_L (°C)	Temperature Lift ΔT (°C)	
			Experimental Results	Theoretical Results
$CaCl_2 \cdot 2NH_3$	105	25	18	19
	120	25	14	17
$CaCl_2 \cdot 4NH_3$	90	25	21	22
	105	30	23	27
	120	30	22	25

small difference between the theoretical results and the experimental results.

It was also found from Table 5 that the temperature lift was smaller in the case of the initial states of $CaCl_2 \cdot 2NH_3$ and $MnCl_2 \cdot 6NH_3$, compared with that for the initial states of $CaCl_2 \cdot 4NH_3$ and $MnCl_2 \cdot 6NH_3$. This was due to the fact that at the same T_M, the decomposition pressure was higher for the reaction of $CaCl_2 \cdot 4/8NH_3$. During the high pressure process P_H in the system operation, the salt of $CaCl_2$ was decomposed and the salt of $MnCl_2$ was synthesized. Since the synthesis pressure of $MnCl_2$ is the same as the decomposition pressure of $CaCl_2$, as shown in Figure 1b, the synthesis temperature of $MnCl_2$ was then higher for the initial states of $CaCl_2 \cdot 4NH_3$ and $MnCl_2 \cdot 6NH_3$. Thus, the temperature lift ΔT was larger in this case.

The main focus of this article was the solid–gas reaction in the heat transformer system. The results of the reaction degrees x_{24}, x_{48}, and x_{26} are shown in Figure 8. The left and right dotted lines in Figure 8a represent time 1 (at about 5000 s) and time 2 (at about 15,000 s), respectively; while the left and right dotted lines in Figure 8b represent time 3 (at about 7000 s) and time 4 (at about 23,000 s), respectively.

The molar contents of $CaCl_2 \cdot 2NH_3$, $CaCl_2 \cdot 4NH_3$, and $CaCl_2 \cdot 8NH_3$ at each time are shown in Figure 8c. At times 1 and 2, the salt of $CaCl_2$ is mainly in the form of $CaCl_2 \cdot 2NH_3$ and $CaCl_2 \cdot 4NH_3$, respectively. The fraction of $CaCl_2 \cdot 8NH_3$ in the reactive block with $CaCl_2$ is small. Therefore, the main reaction in the case shown in Figure 8a was the reaction of $CaCl_2 \cdot 2/4NH_3$. Similar to the results at time 1 and 2, the major fraction of the salt of $CaCl_2$ at times 3 and 4 was $CaCl_2 \cdot 4NH_3$ and $CaCl_2 \cdot 8NH_3$, respectively. Thus, the main reaction in the case shown in Figure 8b was the reaction of $CaCl_2 \cdot 4/8NH_3$.

In addition to the main reaction discussed above, the other reaction between $CaCl_2$ and NH_3 in the cases shown in Figures 8a, b was also found. Therefore, it was concluded that the reactions of $CaCl_2 \cdot 2/4NH_3$ and $CaCl_2 \cdot 4/8NH_3$ might occur simultaneously in the solid–gas reaction heat transformer system. It was then necessary to investigate the favored conditions for the simultaneous occurrence of multistep reactions between $CaCl_2$ and NH_3. In this article, the investigated conditions included the driving temperature T_M and the ambient temperature T_L, the relative gas volume V_g/V_B and the initial charging pressure P_0, the specific heat transfer area A/V_B and the heat transfer coefficient U_{Mn} of $MnCl_2$ during synthesis process. The impacts of the simultaneous occurrence of multistep reactions on the system performance indicators, which included the temperature lift ΔT, specific power, and system COP, were also investigated.

Favored conditions for the simultaneous occurrence of multistep reactions

As mentioned earlier, the system operation was composed of two processes: the high pressure process P_H and the low pressure process P_L. In the high pressure process P_H, $CaCl_2$ was decomposed and $MnCl_2$ was synthesized; and in the low pressure process P_L, $MnCl_2$ was decomposed and $CaCl_2$ was synthesized. For simplicity, each process was stopped when the reaction degree x reached 0.9 in synthesis or 0.1 in decomposition. The parameters are listed in Table 6, except for those specifically mentioned.

The variation ranges of the reaction degrees x_{24} and x_{48} during the system operation were defined as Δx_{24} and Δx_{48}, respectively. The main reaction between $CaCl_2$ and NH_3 in each system with the initial states of $CaCl_2 \cdot 2NH_3$ and $CaCl_2 \cdot 4NH_3$ was designated as the reaction of $CaCl_2 \cdot 2/4NH_3$ and $CaCl_2 \cdot 4/8NH_3$, respectively. Thus, for the solid–gas reaction heat transformer system designed with the reaction of $CaCl_2 \cdot 2/4NH_3$, the larger Δx_{48} implied more obvious occurrence of the reaction of $CaCl_2 \cdot 4/8NH_3$. Consequently, the simultaneous occurrence of multistep reactions was more obvious. For the system designed for the reaction of $CaCl_2 \cdot 4/8NH_3$, the larger Δx_{24} implied more obvious occurrence of multistep reactions. The effects of several parameters on Δx_{24} and Δx_{48} were then investigated.

Effects of T_M *and* T_L. The driving temperature T_M of the solid–gas reaction heat transformer system was designed at 90–120°C. The ambient temperature T_L was designed at 0–30°C. The influence of T_M on the reaction was investigated, and the results are shown in Figure 9. For the initial state of $CaCl_2 \cdot 2NH_3$, the reaction degree x_{48} is shown in Figure 9a, and Δx_{48} is shown in Figure 9b. The results for the case of the initial state of $CaCl_2 \cdot 4NH_3$ are shown in Figures 9c, d.

It was concluded from Figures 9a, b that the amount of the reaction of $CaCl_2 \cdot 4/8NH_3$ was small when T_M was lower than 105°C. When T_M was higher than 105°C, Δx_{48} increased with T_M. However, for the initial state of $CaCl_2 \cdot 4NH_3$, Δx_{24} increases with T_M, as shown in Figures 9c, d.

In the solid–gas reaction heat transformer system, the synthesis of $CaCl_2$ at T_L accompanied the decomposition of $MnCl_2$ at T_M. The decomposition pressure of $MnCl_2$ was the same as the synthesis pressure of $CaCl_2$. It was concluded

Table 6. Parameters Used in the Theoretical Analysis

T_M (°C)	T_L (°C)	V_g/V_B	P_0 (MPa)	A/V_B (m^2/m^3)	U_{Mn} [W/(m^2 °C)]
120	30	0.2	0.6	100	50

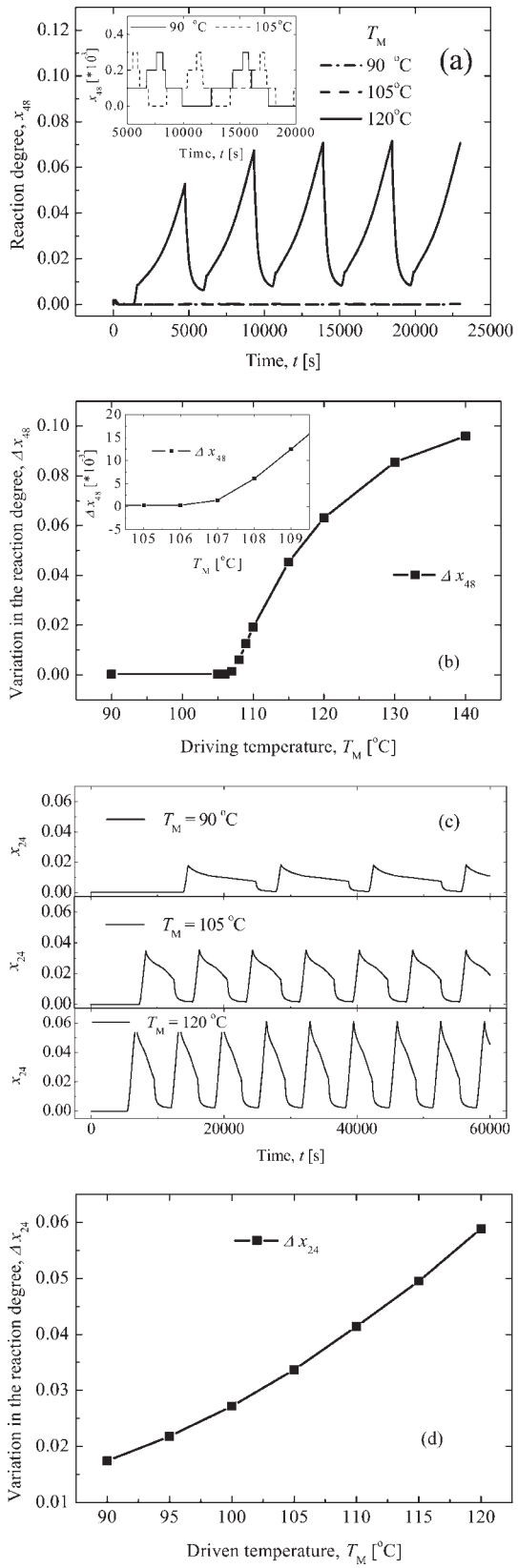

Figure 9. Reaction degrees at different T_M.

(a, b) for the initial state of $CaCl_2 \cdot 2NH_3$; (c, d) for the initial state of $CaCl_2 \cdot 4NH_3$ (the ambient temperature T_L was 30°C).

from Figure 4 that the equilibrium pressure P_{eq48} of the reaction of $CaCl_2 \cdot 4/8NH_3$ at T_L was higher than the equilibrium pressure P_{eq24} of the reaction of $CaCl_2 \cdot 2/4NH_3$. The decomposition temperature T_M of $MnCl_2$ should be then higher for the synthesis of the reaction of $CaCl_2 \cdot 4/8NH_3$, compared to T_M for the synthesis of the reaction of $CaCl_2 \cdot 2/4NH_3$. Therefore, when T_M was lower than 105°C, only the reaction of $CaCl_2 \cdot 2/4NH_3$ happened in the solid–gas reaction heat transformer system. When T_M was higher than 105°C, the reaction of $CaCl_2 \cdot 4/8NH_3$ could also be found in the system, as shown in Figures 9a, b.

As shown in Table 2, the temperatures of the heat transfer fluids for the reactors with $MnCl_2$ and $CaCl_2$ during the high pressure process P_H were both T_M. For the initial state of $CaCl_2 \cdot 4NH_3$, the decompositions of the reactions of $CaCl_2 \cdot 2/4NH_3$ and $CaCl_2 \cdot 4/8NH_3$ occurred simultaneously in the system. With the increase of T_M, the decomposition rate of the reaction of $CaCl_2 \cdot 2/4NH_3$ increased. Therefore, Δx_{24} increases with T_M, as shown in Figure 9d.

The decomposition rates of $MnCl_2$ and $CaCl_2$ increased with the driving temperature T_M. Thus, it was found in Figure 9c that in the same period, the system with T_M at 90°C finished four cycles, while the system with T_M at 120°C finished about nine cycles. Therefore, the cycle period of solid–gas reaction heat transformer system could be shortened with higher T_M.

The effects of the ambient temperature T_L on the simultaneous occurrence of multistep reactions between $CaCl_2$ and NH_3 were also investigated. The results for the initial state of $CaCl_2 \cdot 2NH_3$ are shown in Figure 10a and the results for the initial state of $CaCl_2 \cdot 4NH_3$ are shown in Figure 10b. It was found that the ambient temperature T_L has little influence on Δx_{24} for the initial state of $CaCl_2 \cdot 4NH_3$. However, Δx_{48} decreased with T_L for the initial state of $CaCl_2 \cdot 2NH_3$, as indicated in Figure 10a.

Effects of V_g/V_B and P_0. Δx_{24} for the reaction of $CaCl_2 \cdot 2/4NH_3$ and Δx_{48} for the reaction of $CaCl_2 \cdot 4/8NH_3$ under different relative gas volume V_g/V_B and different initial charging pressure P_0 are depicted in Figure 11. The effect of the relative gas volume is shown in Figure 11a. It was found that Δx_{24} for the initial state of $CaCl_2 \cdot 4NH_3$ and Δx_{48} for the initial state of $CaCl_2 \cdot 2NH_3$ both increased with the relative gas volume. The increase of Δx_{48} was mainly due to the increment of gas amount in the gas tank shown in Figure 6. As there was more gas initially charged in the solid–gas heat transformer system, more NH_3 was available for the synthesis of the reaction of $CaCl_2 \cdot 4/8NH_3$. Thus, Δx_{48} increased. Comparing the curve of Δx_{24} with that of Δx_{48}, it was found that the effect of the relative gas volume on Δx_{24} was more obvious. Δx_{24} at the relative gas volume of 0.5 was about 0.15, while Δx_{24} at the relative gas volume of 4 and 5 was almost 1.0. Therefore, for the initial state of $CaCl_2 \cdot 4NH_3$, the multistep reactions between $CaCl_2$ and NH_3 occurred simultaneously in the solid–gas reaction heat transformer system at large V_g/V_B. The reaction between $CaCl_2$ and NH_3 in the system should be described as from $CaCl_2 \cdot 2NH_3$ to $CaCl_2 \cdot 8NH_3$. Obviously, this was different from the designed condition for the system operation, which was from $CaCl_2 \cdot 4NH_3$ to $CaCl_2 \cdot 8NH_3$. Thus, the multistep reactions between $CaCl_2$ and NH_3 should be taken into consideration for the system design.

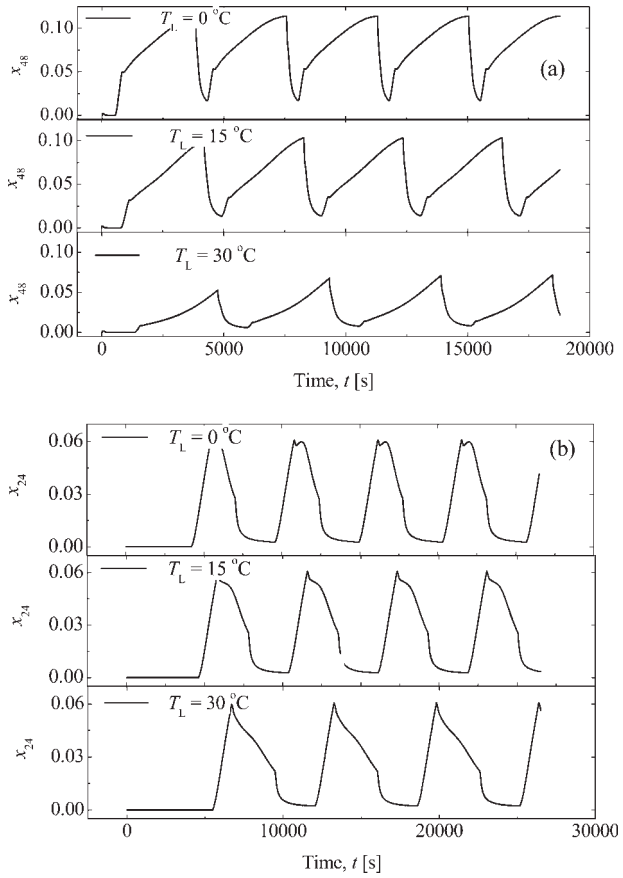

Figure 10. Reaction degrees at different T_L.

(a) For the initial state of $CaCl_2 \cdot 2NH_3$; (b) for the initial state of $CaCl_2 \cdot 4NH_3$ (the driving temperature T_M was 120°C).

The larger Δx_{24} in the system with larger V_g/V_B was due to the faster decomposition rate of $CaCl_2$. As shown in Ref. 9, the cycle period of the solid–gas reaction heat transformer with larger relative gas volume is shorter. It was also concluded in Ref. 9 that the balance effect of gas volume on the reaction rates of $MnCl_2$ and $CaCl_2$ was weaker at larger relative gas volume. Since the balance effect led to increasing synthesis rate of $CaCl_2$ and decreasing decomposition rate of $MnCl_2$,[9] the decomposition rate of $CaCl_2$ was faster at larger relative gas volume. Therefore, Δx_{24} increases, as shown in Figure 11a.

The effects of the initial charging pressure P_0 on Δx_{24} and Δx_{48} are shown in Figure 11b. For the initial state of $CaCl_2 \cdot 2NH_3$, Δx_{48} increased with the initial charging pressure P_0; while for the initial state of $CaCl_2 \cdot 4NH_3$, Δx_{24} decreased with P_0. Since high gas pressure P was favored for the synthesis of the reaction of $CaCl_2 \cdot 4/8NH_3$ and low gas pressure P was favored for the decomposition of the reaction of $CaCl_2 \cdot 2/4NH_3$, Δx_{48} was larger at higher P_0, and Δx_{24} was larger at lower P_0.

Effects of A/V_B *and* U_{Mn}. Figure 12 depicts the effects of the specific heat transfer area A/V_B and the heat transfer coefficient U_{Mn} on Δx_{24} and Δx_{48}. Since the performance of heat transfer was improved with larger specific heat transfer area, the salt temperature T_s was closer to the temperature of the heat transfer fluid, and the reaction rate was faster. Therefore, it was found from Figure 12a that both Δx_{24} and Δx_{48} increase with the specific heat transfer area.

As the heat transfer performance of the reactor with $MnCl_2$ is also improved with larger U_{Mn}, the salt temperature T_M during synthesis was closer to the temperature of the heat transfer fluid at larger U_{Mn}. Thus, the synthesis rate of $MnCl_2$ was faster. As the relative gas volume in Figure 12b was 0.2, the balance effect of gas volume on the reaction rates of $MnCl_2$ and $CaCl_2$ was strong. Therefore, the decomposition rate of $CaCl_2$ was also increased at larger U_{Mn}. Correspondingly, Δx_{24} was larger. However, for the initial state of $CaCl_2 \cdot 2NH_3$, the synthesis of the reaction of $CaCl_2 \cdot 4/8NH_3$ accompanied the decomposition of $MnCl_2$. Because the conditions for the synthesis of $CaCl_2$ and the decomposition of $MnCl_2$ were not influenced by U_{Mn}, Δx_{48} did not

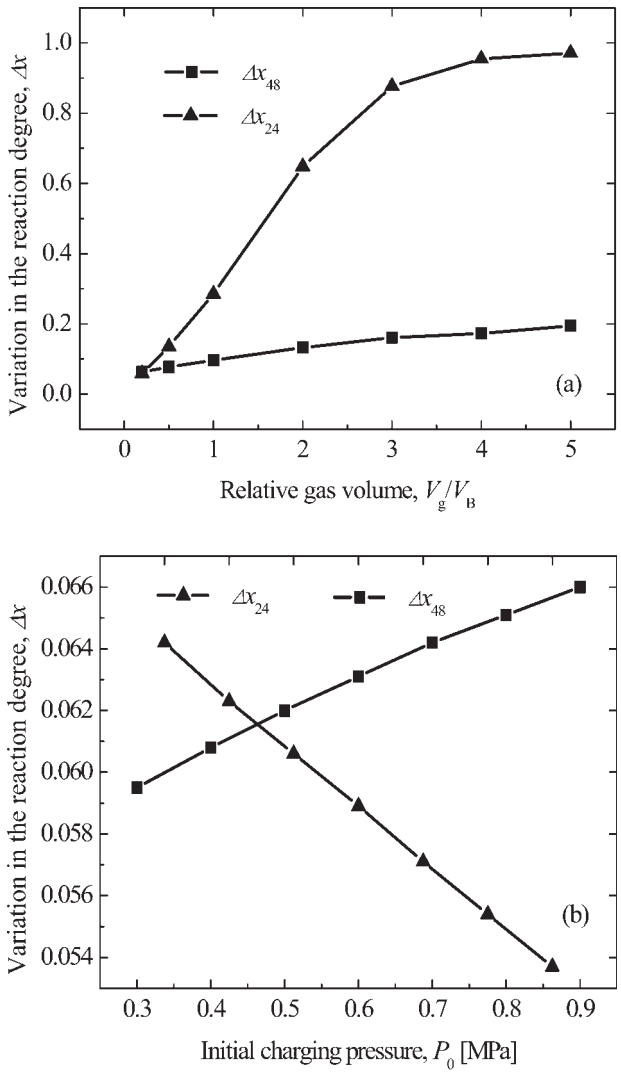

Figure 11. Variations of Δx_{24} and Δx_{48}.

(a) Under different relative gas volume (the initial charging pressure P_0 was 0.6 MPa); (b) under different initial charging pressure (the relative gas volume was 0.2).

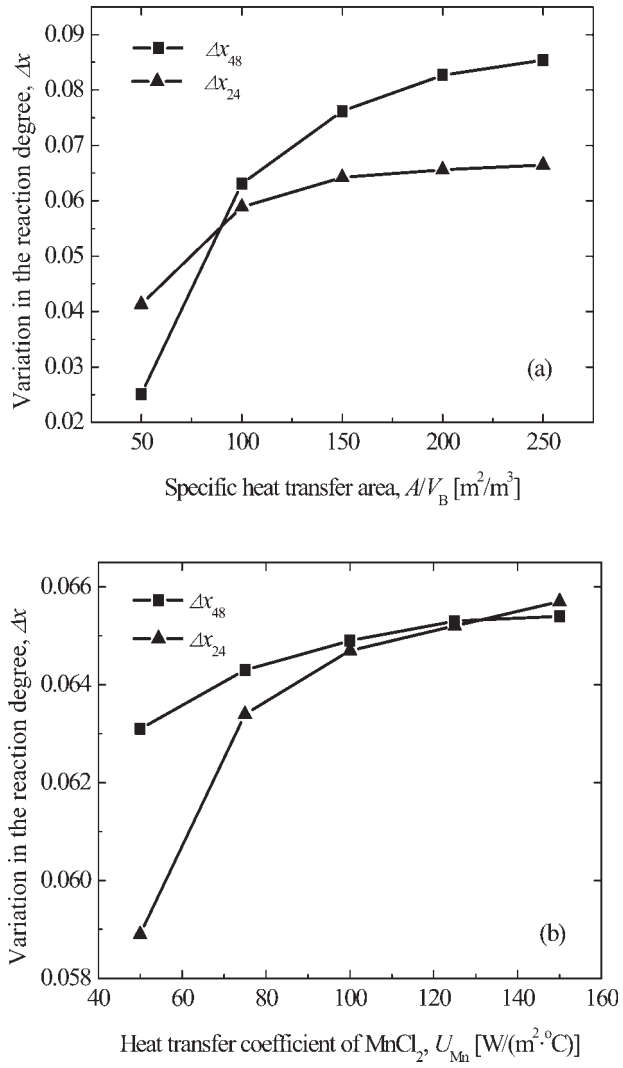

Figure 12. Variations of Δx_{24} and Δx_{48}.

(a) Under different specific heat transfer area (the heat transfer coefficient U_{Mn} of $MnCl_2$ during synthesis was 50 W/(m^2 °C)); (b) under different heat transfer coefficient of $MnCl_2$ (the specific heat transfer area was 100 m^2/m^3).

change a lot. As shown in Figure 12b, Δx_{48} at U_{Mn} of 50 W/(m^2 °C) is about 0.063; and Δx_{48} at U_{Mn} of 150 W/(m^2 °C) is about 0.0655.

From Figures 9–12, it was concluded that the relative gas volume has the most significant effect on the simultaneous occurrence of multistep reactions between $CaCl_2$ and NH_3. With higher driving temperature T_M, the simultaneous occurrence of multistep reactions was more obvious for the initial state of $CaCl_2{\cdot}4NH_3$. For the initial state of $CaCl_2{\cdot}2NH_3$, the reaction of $CaCl_2{\cdot}4/8NH_3$ did not happen when the driving temperature T_M was lower than 105°C. When the temperature T_M was higher than 105°C, Δx_{48} increased with T_M. With the increase of the specific heat transfer area, the heat transfer performance was improved. Therefore, the temperature of the reactive block with the salt was closer to that of the heat transfer fluid. The reaction was then faster and Δx_{24} and Δx_{48} were larger. The favored conditions for the simultaneous occurrence of multistep reactions between $CaCl_2$ and NH_3 in the cases of the initial states of $CaCl_2{\cdot}2NH_3$ and $CaCl_2{\cdot}4NH_3$ are summarized in Table 7.

Impact of the simultaneous occurrence of the reactions of $CaCl_2{\cdot}2/4NH_3$ and $CaCl_2{\cdot}4/8NH_3$ on the performance of the solid–gas reaction heat transformer system

The impact of the simultaneous occurrence of multistep reactions on the performance of the solid–gas reaction heat transformer system was investigated. The system performance indicators were first calculated without the consideration of multistep reactions, where the single reaction between $CaCl_2$ and NH_3 was supposed. The system performance indicators were also calculated with the consideration of multistep reactions. The differences revealed the impact of the simultaneous occurrence of multistep reactions.

The conditions investigated in this article are listed in Table 8. Under Conditions 1A and 2A, only the reaction of $CaCl_2{\cdot}2/4NH_3$ was considered. Under Conditions 3A and 4A, only the reaction of $CaCl_2{\cdot}4/8NH_3$ was considered. The simultaneous occurrence of multistep reactions between $CaCl_2$ and NH_3 was then considered under other conditions. The parameters for each condition are also listed in Table 8. The driving temperature T_M was 120°C, and the heat transfer coefficient U_{Mn} of $MnCl_2$ during synthesis process was 50 W/(m^2 °C).

The Case of the Initial State of $CaCl_2{\cdot}2NH_3$. The variations of the salt temperature T_s and the reaction degree x are depicted in Figure 13. The results of T_s under Condition 1A are shown in Figure 13a. The results of T_s and x under Condition 1B are shown in Figures 13b, c, respectively. The results under Conditions 2A and 2B are shown in Figures 13d–f. Since the results under Conditions 1A and 2A are based on the single reaction assumption, which has been discussed in Ref. 9, the variations of the reaction degree x were not shown in this article.

From Figure 13, it was concluded that there was almost no reaction of $CaCl_2{\cdot}4/8NH_3$ under Condition 2B; while there was obvious occurrence of the reaction of $CaCl_2{\cdot}4/8NH_3$ under Condition 1B. It was also found in Figure 13 that the results of the salt temperatures T_{Mn} and T_{Ca} under Conditions 2A and 2B were the same, while those under Conditions 1A and 1B were different. The difference of the results under Conditions 1A and 1B was therefore due to the simultaneous

Table 7. Favored Conditions for the Simultaneous Occurrence of Multistep Reactions

Initial State of $CaCl_2$	T_M	T_L	V_g/V_B	P_0	A/V_B	U_{Mn}
$CaCl_2{\cdot}2NH_3$	High	Low	Large	High	High	Almost no effect
$CaCl_2{\cdot}4NH_3$	High	Almost no effect	Large	Low	High	High

Table 8. Parameters in the Conditions Considered

Condition	Initial State of $CaCl_2$	Consideration of Multistep Reactions	T_L (°C)	V_g/V_B	P_0 (MPa)	A/V_B (m^2/m^3)
1A	$CaCl_2 \cdot 2NH_3$	No	0	5	0.9	200
1B		Yes				
2A	$CaCl_2 \cdot 2NH_3$	No	30	0.2	0.3	50
2B		Yes				
3A	$CaCl_2 \cdot 4NH_3$	No	30	5	0.3	200
3B		Yes				
4A	$CaCl_2 \cdot 4NH_3$	No	30	0.2	0.9	50
4B		Yes				

The heat transfer coefficient of $MnCl_2$ during synthesis U_{Mn} was 50 W/(m^2 °C) and the driving temperature T_M was 120°C).

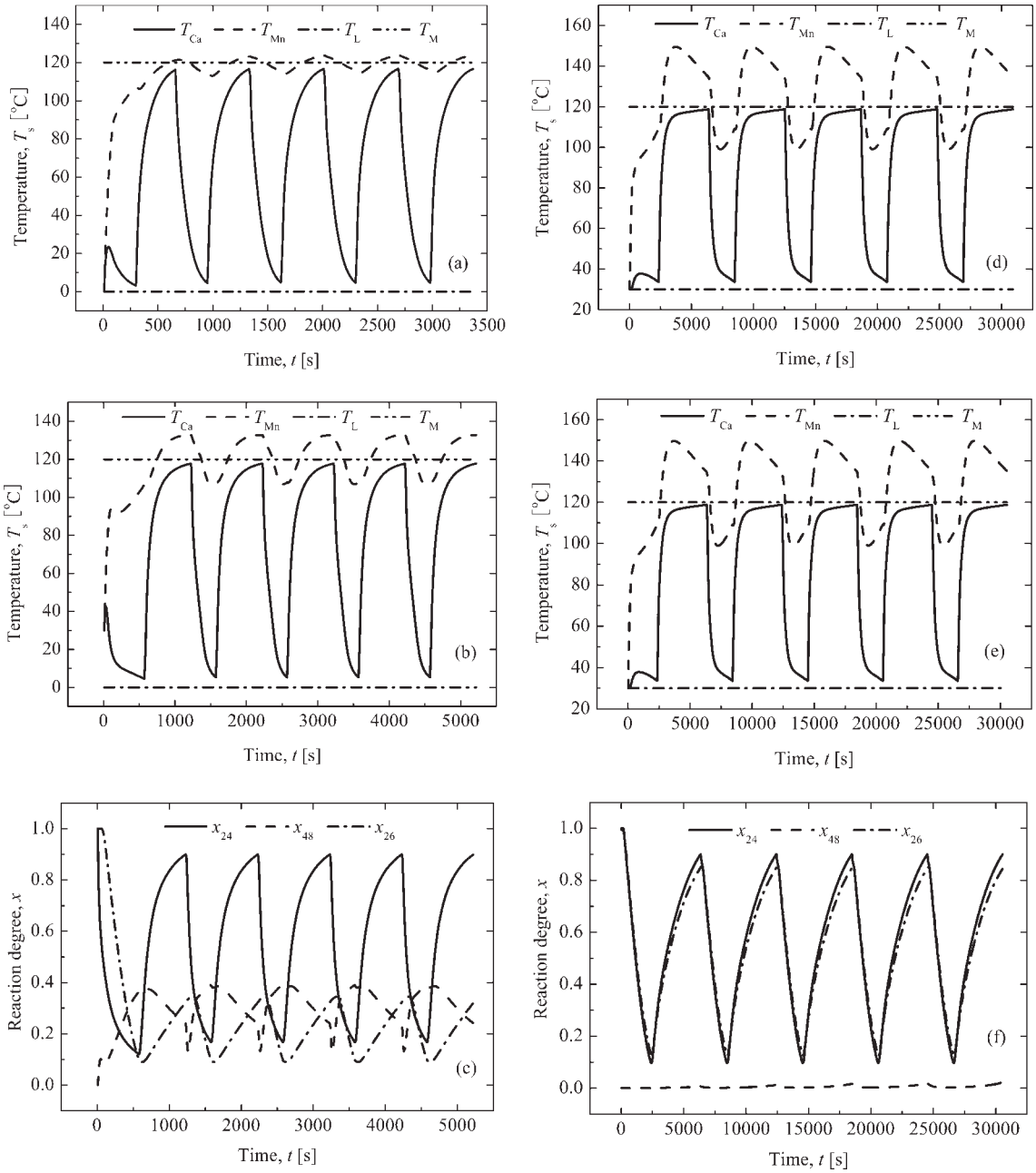

Figure 13. Variations of the salt temperature T_s and the reaction degree x.

(a) The salt temperature T_s under Condition 1A; (b) the salt temperature T_s under Condition 1B; (c) the reaction degree x under Condition 1B; (d) the salt temperature T_s under Condition 2A; (e) the salt temperature T_s under Condition 2B; and (f) the reaction degree x under Condition 2B.

occurrence of multistep reactions. And the results under Condition 2A where no multistep reactions were considered were the same as those under Condition 2B where the multistep reactions were taken into consideration.

Table 9 lists the system performance indicators: the temperature lift ΔT, specific power, and system COP, which were determined by Eq. 11. The results under Conditions 2A and 2B were almost the same, and there was obvious difference between the results under Conditions 1A and 1B.

$$\text{Specific power} = \frac{\left[\int U \cdot A \cdot (T_{\text{Mn}} - T_{\text{f}}) \cdot dt\right]_{\text{syn}}}{m_{\text{B}} \cdot \left[\int dt\right]_{\text{syn}}} \tag{11a}$$

$$\text{COP} = \frac{\left[\int U \cdot A \cdot (T_{\text{Mn}} - T_{\text{f}}) \cdot dt\right]_{\text{syn}}}{\left[\int U \cdot A \cdot (T_{\text{f}} - T_{\text{Ca}}) \cdot dt\right]_{\text{dec}} + \left[\int U \cdot A \cdot (T_{\text{f}} - T_{\text{Mn}}) \cdot dt\right]_{\text{dec}}} \tag{11b}$$

From Table 9, it was also concluded that the system performance could be improved by selecting proper system structure and operation conditions. For the initial state of $CaCl_2{\cdot}2NH_3$, neglecting the reaction of $CaCl_2{\cdot}4/8NH_3$ might lead to underestimation of the system performance.

The Case of the Initial State of $CaCl_2{\cdot}4NH_3$. The system performance for the initial state of $CaCl_2{\cdot}4NH_3$ is summarized in Table 10. Under Condition 4B, no significant occurrence of the reaction of $CaCl_2{\cdot}2/4NH_3$ was found; while it was obvious under Condition 3B. Since in category A, only the single reaction was considered; while in category B, the multistep reactions between $CaCl_2$ and NH_3 were taken into consideration; the results under Condition 4B were similar to those under Condition 4A, and the results under Condition 3B were different from those under Condition 3A. The figures in this case are similar to those in Figure 13 and were not shown in this article.

It was concluded from Table 10 that the specific power was smaller when the reaction of $CaCl_2{\cdot}2/4NH_3$ happened. It was also concluded that, with a proper design of solid–gas reaction heat transformer system, the temperature lift ΔT could be improved from 14°C (under Condition 3B) to 32°C (under Condition 4B), and the system COP could be improved from 0.27 (under Condition 3B) to 0.334 (under Condition 4B). The smaller specific power under Condition 4B was due to the longer cycle period at small relative gas volume of 0.2, where the balance effect of the gas volume on the reaction rates of $MnCl_2$ and $CaCl_2$ was strong, as concluded in Ref. 9.

Table 9. The System Performance Indicators Under Conditions 1A and 1B, 2A and 2B

Condition	Temperature Lift ΔT (°C)	Specific Power/W/kg of Block with $MnCl_2$	System COP
1A	4	70	0.004
1B	13	322	0.045
2A	30	189	0.237
2B	30	190	0.243

Table 10. The System Performance Indicators Under Conditions 3A and 3B, 4A and 4B

Condition	Temperature Lift ΔT (°C)	Specific Power/W/kg of Block with $MnCl_2$	System COP
3A	13	380	0.145
3B	14	269	0.270
4A	37	202	0.372
4B	32	188	0.334

Conclusion

The performance of the solid–gas reaction heat transformer system was theoretically and experimentally investigated. The heat transformer system was single-stage system and comprised of $MnCl_2$ and $CaCl_2$ as the reactive salt and NH_3 as the reactive gas. The reaction between $MnCl_2$ and NH_3 was $MnCl_2{\cdot}2/6NH_3$, while the reaction between $CaCl_2$ and NH_3 could be $CaCl_2{\cdot}2/4NH_3$ and $CaCl_2{\cdot}4/8NH_3$. The possible simultaneous occurrence of multistep reactions between $CaCl_2$ and NH_3 was considered in the theoretical analysis. The results in theoretical analysis were compared with those in experiments, and the theoretical results agreed well with the experimental results.

It was concluded that the two reactions between $CaCl_2$ and NH_3 might occur simultaneously in the solid–gas reaction heat transformer system. For the initial states of $CaCl_2{\cdot}2NH_3$ and $CaCl_2{\cdot}4NH_3$, high driving temperature, large relative gas volume, and large specific heat transfer area would lead to more obvious occurrence of the reaction of $CaCl_2{\cdot}4/8NH_3$ and $CaCl_2{\cdot}2/4NH_3$, respectively. For the initial state of $CaCl_2{\cdot}2NH_3$, the reaction of $CaCl_2{\cdot}4/8NH_3$ only occurred when T_{M} was higher than 105°C. The favored initial charging pressure P_0 for the simultaneous occurrence of the multistep reactions between $CaCl_2$ and NH_3 was different in the cases of the initial states of $CaCl_2{\cdot}2NH_3$ and $CaCl_2{\cdot}4NH_3$. High P_0 was favored in the former case; while low P_0 was favored in the latter case.

The effects of the simultaneous occurrence of multistep reactions on the system performance were also investigated in this article. The system performance indicators were the temperature lift ΔT, specific power, and system COP. It was concluded that for the initial state of $CaCl_2{\cdot}2NH_3$, the occurrence of the reaction of $CaCl_2{\cdot}4/8NH_3$ led to larger temperature lift ΔT, larger specific power, and larger system COP. However, for the initial state of $CaCl_2{\cdot}4NH_3$, the occurrence of the reaction of $CaCl_2{\cdot}2/4NH_3$ would lead to smaller specific power.

The system performance for the initial state of $CaCl_2{\cdot}4NH_3$ was better than those for the initial state of $CaCl_2{\cdot}2NH_3$. Therefore, it was better to design the solid–gas reaction heat transformer system with the reactions of $MnCl_2{\cdot}2/6NH_3$ and $CaCl_2{\cdot}4/8NH_3$. Moreover, the system performance could be improved by selecting proper system structure and operation conditions.

Acknowledgments

The authors would like to express their gratitude to S.L. Li, Y.Q. Yu, and Z.W. Ma for assistance. This research was financially supported by

Shanghai Pujiang Program (06PJ14061) and Shanghai Municipal Science and Technology Committee (06SR07106).

Notation

a = constant (1/s)
A = heat transfer area (m^2)
b = constant
C = heat capacity [J/(kg °C)]
COP = coefficient of performance
f = mass fraction
H = enthalpy change (J/mol)
k = gas permeability (m^2)
m = mass (kg)
MV = molar volume (m^3/mol)
MW = molar weight (kg/mol)
n = molar amount (mol)
P = pressure (MPa)
R = gas constant [J/(mol °C)]
s = source term (W)
S = entropy change [J/(mol °C)]
t = time (s)
T = temperature (°C)
U = heat transfer coefficient [W/(m^2 °C)]
V = volume (m^3)
x = reaction degree

Greek letters

Δ = difference
ε = porosity
ρ = density (kg/m^3)
v = molar ratio of gas to solid

Subscripts

0 = initial charging
24 = $CaCl_2 \cdot 2/4NH_3$
48 = $CaCl_2 \cdot 4/8NH_3$
26 = $MnCl_2 \cdot 2/6NH_3$
b = apparent value
f = heat transfer fluid
B = reactive block
Ca = $CaCl_2$
dec = decomposition
eq = equilibrium
g = gas
G = expanded graphite
H = high
L = low
M = medium
Mn = $MnCl_2$
s = salt
syn = synthesis

Literature Cited

1. Wang RZ, Li Y. Perspectives for natural working fluids in China. *Int J Refrig*. 2007;4:568–581.
2. Ziegler F. State of the art in sorption heat pumping and cooling technologies. *Int J Refrig*. 2002;25:450–459.
3. Kang BH, Yabe A. Performance analysis of a metal-hydride heat transformer for waste heat recovery. *Appl Therm Eng*. 1996;16:677–690.
4. Wang C, Zhang P, Yu YQ, Wang RZ. Conceptual design of novel multi-stage solid-gas heat transformer system. In: *Proceedings of the 22nd IIR International Congress of Refrigeration*, Beijing, China, 2007.
5. Wang C, Zhang P, Wang RZ. Temperature profile during gas-solid reaction within reactor for heat transformer. *J Chem Ind Eng*. 2007;58:310–316 (in Chinese).
6. Yu YQ, Zhang P, Wu JY, Wang RZ. Energy upgrading by solid-gas reaction heat transformer: a critical review. *Renew Sustain Energy Rev*. 2008;12:1302–1324.
7. Castaing J, Neveu P. Development of a numerical sizing tool applied to a solid-gas thermochemical transformer. *Appl Therm Eng*. 1997; 17:501–536.
8. Klein HP, Groll M. Heat transfer characteristics of expanded graphite matrices in metal hydride beds. *Int J Hydrogen Energy*. 2004; 29:1503–1511.
9. Zhang P, Wang C, Wang RZ. Composite reactive block for heat transformer system and improvement of system performance. *J Chem Eng Jpn*. 2007;40:1275–1280.
10. Olives R, Mauran S. A highly conductive porous medium for solid-gas reactions: effect of the dispersed phase on the thermal tortuosity. *Trans Porous Media*. 2001;43:377–394.
11. Han JH, Cho KW, Lee KH, Kim H. Porous graphite matrix for chemical heat pump. *Carbon*. 1998;36:1801–1810.
12. Oliveira RG. Consolidated composite reactive bed for refrigeration sorption system. Post-doctor report, Shanghai Jiao Tong University. 2006:10–12.
13. Mazet N, Amouroux M, Spinner B. Analysis and experimental study of the transformation of non-isothermal solid/gas reacting medium. *Chem Eng Commun*. 1991;99:155–174.
14. Lebrun M. Models of heat and mass transfers in solid/gas reactor used as chemical heat pumps. *Chem Eng Sci*. 1990;45:1743–1753.
15. Spinner B, Rhault F. Kinetics models in solid/gas reactions under imposed pressure and temperature constraints. In *Proceedings of International Workshop on Heat Transformation and Storage,* Ispra, Italy, 1985.
16. Han JH, Lee KH, Kim DH, Kim H. Transformation analysis of thermochemical reactor based on thermophysical properties of graphite-$MnCl_2$ complex. *Ind Eng Chem Res*. 2000;39:4127–4139.
17. Li SL, Wu JY, Xia ZZ. Study of the adsorption performance of composite adsorbent of $CaCl_2$ and expanded graphite with ammonia as adsorbate. In: *Proceedings of the 22nd IIR International Congress of Refrigeration*, Beijing, China, 2007.

Manuscript received Jan. 11, 2008, and revision received Apr. 25, 2008.